Chapter 14

Photocatalytic TiO_2: From Airless Jet Spray Technology to Digital Inkjet Printing

Claudia L. Bianchi, Carlo Pirola, Marta Stucchi,
Giuseppina Cerrato, Federico Galli,
Alessandro Di Michele, Serena Biella,
Wen-Fan Chen, Pramod Koshy, Charles Sorrell and
Valentino Capucci

Additional information is available at the end of the chapter

http://dx.doi.org/10.5772/intechopen.72790

Abstract

TiO_2 powders can be employed as both photocatalytic and structural materials, leading to applications in external coatings or in interior furnishing devices, including cement mortar, tiles, floorings, and glass supports. The technology of photocatalytic building materials is connected with the widespread production of photocatalytic active tiles. All the techniques proposed in the study involve the employment of nanosized TiO_2: this represents a new problem to be dealt with, as inhaling nanoparticles exposes workers during industrial production and people in everyday locations to their dangerousness. Only very recently the employment of microsized TiO_2 has been proposed, and the authors in this manuscript report the use of micrometric titania materials, but employing a new deposition technique, which is digital inkjet printing. It represents an improvement of the classical spray coating methods, as it requires piezoelectric heads to precisely direct the deposition of the suspension with an electrostatic field. The mixture contains aqueous/organic components containing micrometric TiO_2: to form a suspension, which is printed onto the surface of porcelain grès, large slabs using a digital printer. Many advantages are immediately evident, namely rapid and precise deposition, (almost) no waste of raw materials, thereby highlighting the economy, environmental friendliness, and sustainability of the process. All the materials we obtained have been thoroughly characterized by means of several experimental physico-chemical techniques, such as Raman microspectroscopy and scanning electron microscopy coupled with elemental analysis. Two different model VOCs, ethanol and toluene, and NOx have been selected to test the

photocatalytic performances of the abovementioned tiles. Moreover, the antibacterial properties of the tiles have been determined, using E*scherichia* coli as example. Life cycle assessments (LCAs) for the two processes were modeled for 1 m^2 of tiles produced in Modena, Italy. The impact assessments revealed that jet spraying exhibited uniformly greater impacts than digital inkjet printing and that the principal impacts were in human toxicity, cancer effects, freshwater ecotoxicity, and climate change. Most of the impacts were associated with the energy required for the production processes. Further considerations revealed that jet spraying is projected to generate twice as much CO_2 and 30% more NOx than digital inkjet printing.

Keywords: TiO_2, titania, digital inkjet printing, jet spraying, VOCs, NO_x, E. coli, life cycle assessment, impact assessments

1. Introduction

1.1. Pollution

The WHO (World Health Organization) estimates that 12.6 million deaths each year are attributable to unhealthy environments [1], confirming the urgent need for investment in strategies to reduce environmental risks in cities, homes, and workplaces. Of these deaths, 4.3 million (34%) and 3.7 million (29%) have been linked to exposure to indoor and outdoor pollution, respectively [2]. More broadly, it is considered that 92% of the population lives in areas that are exposed to respirable particulate matter of <2.5 μm in diameter ($PM_{2.5}$) at an annual mean concentration of >10 μg/m^3 (or a 24 h mean of >25 μg/m^3), which exceeds the WHO Air Quality Guidelines (AQG). The worst affected areas are China, the Indian subcontinent, the Middle East, and northern Africa.

Particulate and gaseous air pollution results largely from industrial and motor vehicular sources, although these emissions are exacerbated by those generated by heating [3]. The combustion of solid biomass and impure liquid fuels is the main source of pollution leading to health problems, as evidenced by numerous recent studies. For example, in Ethiopia, the average concentration of respirable particulate matter of diameter of <$PM_{2.5}$ reaches as high as a 24-h mean concentration of 280 μg/m^3, indoor CO levels are greater than the regulatory limits for the US, and the average NO_2 level is 97 ppb [4]. In Southeast Asia, the large-scale burning of biomass causes heavy emissions of combustion by-products, which photochemically transform to other more dangerous molecules [5], such as polycyclic aromatic hydrocarbons (PAHs) [6]. Europe is affected mainly by emissions of nitrogen oxides (NO_x) [7]. Although outdoor pollution tends to be a focal point, indoor air in the US can be two to five times more harmful than outdoor air [8]. Almost 96% of houses in North America are reported to have at least one indoor air quality problem [9]. Cigarette smoke contains more than 7000 chemicals, of which 69 are known to be carcinogenic and many more to be poisonous [10]. Household items, such as cleaning products, air fresheners, and sanitation products, also contribute to indoor pollution by releasing chemicals. Consequently, there are environmental health imperatives to develop technologies that address these while satisfying other demands in the areas of energy efficiency, economic efficiency, utility, and esthetics.

1.2. Photocatalytic TiO_2 and its applications

Semiconductor photocatalysis involves the activation of a photocatalytic material, such as titania (TiO_2), by the action of light to produce charge carriers that undergo redox reactions with water and oxygen molecules [11]. This property allows these materials to decompose organic contaminants ideally into CO_2 and water, thus allowing applications in self-cleaning, anti-fogging, corrosion prevention, and air and water purification [12]. Although there are many scientific and technical requirements for effective photocatalytic performance [13], there are also numerous practical challenges that must be met. One of these is catalyst immobilization [14] because it generally must balance the requirements of achievement of a robust chemical bond to a substrate, the retention of sufficient exposed surface area, and the minimization of contamination from the substrate.

There has been an increase in the sales of TiO_2-based products for self-cleaning and air and water purification owing to growing environmental concerns [15]. One of the key product developments was photocatalytic building materials, which appeared on the market at the beginning of the 1990s [16]. TiO_2 can be applied either in exterior construction or in interior furnishing materials, including concrete, mortar, tiles, flooring, and glass. In the early 2000s, the sales of photocatalytic building materials accounted for ~60% of the total market for photocatalytic materials [17]. Recent market projections to 2020 foreshadow increasing demand in the construction sector for self-cleaning coatings and other technologies for improving air quality, leading to a global market for photocatalyst-based products of ~$2.9 billion [18]. At present, TiO_2-based photocatalyst products constitute 97.6% of the market, and this dominance is a result of TiO_2's low cost, ready availability, and well-documented performance data.

Many studies have demonstrated the effectiveness of photocatalytic materials for pollution abatement of the volatile organic compounds (VOCs) and nitrogen oxides (NO_x) that represent widespread risks to health. For example, concrete paving blocks with TiO_2 added directly to the mix were able to remove 4.01 mg/h/m^2 of NO [19]. However, similar work demonstrated that the efficiency of NO_x photodegradation varied significantly according to preparation method and resultant microstructure, with some products achieving 40% photodegradation while others showed almost no effect [20]. A comparison between pure TiO_2 and TiO_2 embedded in neat hydrated cement revealed that the photocatalytic activity was three to 10 times lower for the latter, which was attributed to the agglomeration of the TiO_2 powder [21]. TiO_2 also has been applied as surface coatings on roofing tiles and corrugated sheet and found to achieve gaseous toluene removal efficiencies as high as 78 $\pm$ 2%, although this was limited by gas concentration and residence time [22].

It is clear that the permanence and performance of TiO_2-containing construction products depend significantly on the method used to immobilize the photocatalyst, whether in the bulk or on the surface. Other factors of importance include the type of substrate and the method of TiO_2 application [23]. Hence, there has been a commensurate focus on the design of such building products and their manufacture in order to obtain maximal lifetimes and efficiencies. An additional consideration is the potential alteration of the photocatalyst by fouling, which can block the active sites and reduce or prevent photocatalysis [24]. Finally, there are also potential health issues associated with the formation of chemical intermediates [25] and the respirability of nanoparticulates [26].

1.3. TiO_2 coatings

One of the most promising areas in photocatalytic building materials is photocatalytically active tiles, which are self-cleaning but also can decompose air pollutants. The standard approach has been to apply TiO_2-based materials on ceramic surfaces and to attempt to immobilize the TiO_2 at as low a temperature as possible. In the case of spray coating of aqueous dispersions of TiO_2 on clay roofing tiles, the heating temperature was 290°C [27]. Chemical vapor deposition (CVD) using gaseous precursors, following by heating at 550°C, also has been investigated [28] but these films suffered from poor adhesion. By contrast, plasma-enhanced chemical vapor deposition (PECVD), involving reheating at 400°C, yielded high-quality materials [29]. Aerosol flame synthesis (temperature probably <700°C) has been used to produce ultra-fine TiO_2 nanoparticles that could be deposited directly on supports [30]. Sol-gel TiO_2 precursors have been coated on cement-based materials by dipping and heating at 500°C [31]. TiO_2 suspensions in water or alcohol also have been sprayed on limestone with no subsequent heating since the porous microstructure immobilized the powder [32]. All of these approaches used nanosized TiO_2.

Although spray coating remains the simplest and least expensive coating technique, recent work [33] reports the functionalization of commercial glazed ceramic tiles with pigment-grade, microsized, anatase (Kronos 1001) using an industrial-type process. This method offers a reduction in the risk of inhalation as it does not involve the use of nanosized TiO_2 powders. The TiO_2 powder was deposited by airless jet spraying aqueous suspensions containing a silica-based commercial product as binder. The tiles were dried and then fired at 680°C in an industrial kiln for 80 min (cold-to-cold cycle).

This work reports a new deposition technique, which is digital inkjet printing. Despite the advantages of conventional spray coating methods, digital inkjet printing offers an advantageous, precise, coating technique that utilizes piezoelectric heads to effect directional deposition of an aqueous/organic ink suspension within an electrostatic field [34]. The suspension contained pigment grade, microsized anatase (Kronos 1077), and this was printed on the surface of porcelain grès *(viz.*, stoneware) tiles using a digital printer. This process has several advantages, including rapid and precise and more uniform deposition and essentially no waste of raw materials, which are favorable for both the economics of the process and the environment. Moreover, with this technique, slabs of large size up to 120 × 360 cm can also be activated. The data for the thin films deposited by digital inkjet printing are contrasted with those for the more conventional method of jet spraying.

2. Materials and methods

2.1. Microsize TiO_2 and porcelain grès tiles

The TiO_2 powder was Kronos 1077, which is ≥98.5% anatase and has a particle size range of 110–130 nm, a BET surface area of 12 m^2/g, a true density of 3800 kg/m^3, and an optical indirect band gap of 3.15 eV [35, 36].

The TiO_2 was deposited on porcelain grès tiles that were manufactured by GranitiFiandre S.p. A. These are dry-pressed tiles fired at 1200–1300°C. The phase assemblage as such consists of glass, mullite, and quartz.

2.2. Digital inkjet printing and airless jet spraying procedures

Conventional, industrial-scale, airless, jet spray deposition was used for the deposition of coatings, as described in brief previously by the authors [37]. However, with the new, innovative, automated decoration of ceramic surfaces by digital instruments, it has become possible to manufacture products of considerably superior quality. Consequently, this work also reports an investigation of the deposition of coatings of photocatalytic TiO_2 by digital inkjet printing using a proprietary ink containing suspended microsized TiO_2 particles.

A prototype digital printer manufactured by Projecta S.p.A. was used to apply the suspensions. Following deposition, the tiles were calcined at 680°C for 80 min using an industrial-scale kiln designed to avoid thermal shock. The cooled tiles then were washed with water, brushed vigorously to remove loose particles, and air jet dried. The process is summarized in **Figure 1**. The water used for degreasing was recovered and purified prior to recycling; any damaged tiles were recycled.

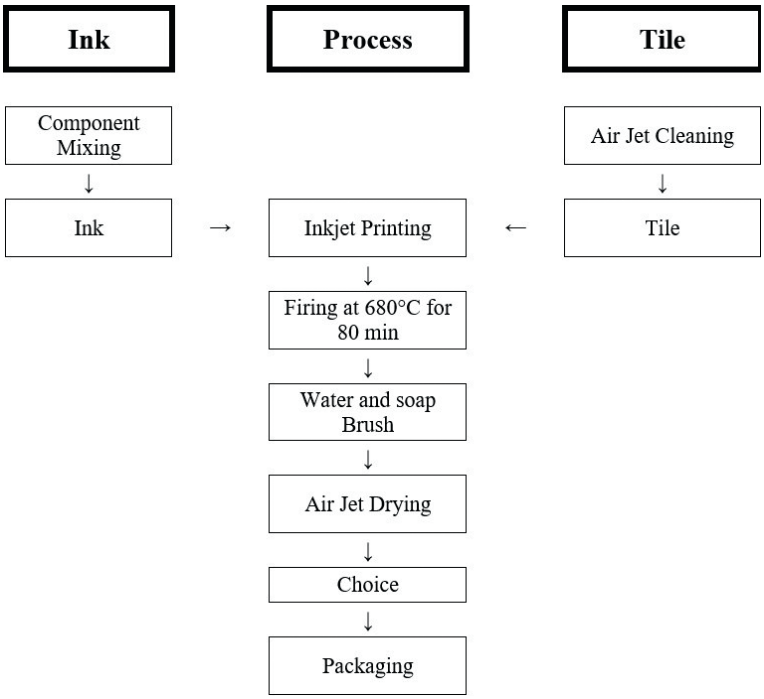

Figure 1. Summary of digital inkjet printing process.

2.3. Characterization

Mineralogical analyses were done by laser Raman microspectroscopy (Raman; inVia Raman Microscope, green laser, 514 nm, 20×, 1.5-μm beam diameter, Renishaw, Wotton-under-Edge, Gloucestershire, UK). Microstructural analyses were done by field emission gun scanning electron microscopy (Field emission gun scanning electron microscopy (FEG-SEM); LEO 1525, 15, or 20 kV accelerating voltage, LEO Electron Microscopy Inc., Thornwood, NY, USA). Elemental analyses were done by paired energy dispersive spectroscopy (EDS; Bruker Quantax, Bruker Italia S.r.l., Milan, Italy).

2.4. Photocatalysis testing

2.4.1. Volatile organic compounds

VOC photodegradation reactions were conducted in a Pyrex glass cylindrical reactor with a diameter of 200 mm and an effective volume of 5 L [38]. A 100-cm^2 digital inkjet-printed sample or jet-sprayed sample was placed at the bottom of the reactor and exposed to a 500-W iron halogen lamp (HG 500, 315–400 nm, UV-A, Jelosil, Milan, Italy). The reactor had two entrances, one for VOC loading and the other for sampling by a gas chromatograph (490 Micro GC System, Agilent Technologies Italia S.p.A, Milan, Italy).

Ethanol and toluene were selected as model pollutants, and the initial concentration for both was 400 ppm for each test. The photodegradation tests were conducted for 6 h.

2.4.2. Nitrogen oxides

Two different setups were used—one under static conditions [39] and the other under flowing conditions [40]. A chemiluminescence NO_x monitor (Teledyne API, Model 200E, San Diego, CA, USA) provided online detection of NO and NO_2 concentrations. The batch reactor consisted of a Pyrex glass cylinder of volume of 25 L; this is described elsewhere [39]. The tile (2 × 20 cm) was located at the bottom of the cylinder and an overhead 500-W iron halogenide lamp (HG 500, 315–400 nm, UV-A, Jelosil, Milan, Italy) provided irradiation of 20 W/m^2. The inlet gas consisted of NO_2 (0.6% in N_2) mixed with air of relative humidity (RH) 40%, which allowed equilibration between NO and NO_2 to be reached quickly. The NO_2 concentration was set at 1000 ppb (static) or 250 ppb (flowing) and tests lasted 6 h each. The continuous flow reactor allowed testing of larger tiles (60 × 60 cm) [40]. A Thermo-Hygro Meter (HT-3006A, Metravi, Calcutta, India) measured both temperature and relative humidity, which ranged between 40 and 50%. Two iron halogen lamps (Jelosil, model HG 500), at 770-mm center-to-center distance, which was designed to irradiate the sample surface with the same 20 W/m^2 light intensity, were used. The total NO_x gas flow was in the range of 140–180 NL/h, which is in accordance with the standard concentration based on the limiting values specified in *Directive 2008/50/EC of the European Parliament and of the Council on Ambient Air Quality and Cleaner Air for Europe* (range 100–200 ppb).

2.5. Antibacterial effects

The photocatalytic tiles were tested using Escherichia coli (E. coli, ATCC 8739) according to *ISO 27447:2009 Fine Ceramics—Test Method for Antibacterial Activity of Semiconducting Photocatalytic Materials*. Each strain was inoculated into a nutrient agar slant, incubated for 16–24 h at 37 ± 1°C, and then transferred to a new nutrient agar slant and again held at 37 ± 1°C for 16–24 h. An appropriate quantity of bacteria was dispersed in 1/500 nutrient broth (NB) to obtain a count of 6.7×10^5 to 2.6×10^6 cells/mL. Tile samples of dimensions 50 × 50 mm were rinsed with distilled water and autoclaved at 121°C for 30 min prior to testing in order to remove any organic residue on the surfaces. For each strain, six tile samples without (controls) and six with photocatalytic coating were investigated. A volume of 0.15 mL of bacterium suspension was placed on each specimen and covered with an inert and non-water adsorbent film of dimensions 40 × 40 mm; the film transmitted >85% of radiation in the range of 340–380 nm. Each specimen was placed in a 100-mm diameter Pyrex Petri dish containing a moistened paper filter to prevent drying of the suspension and covered with a 1-mm thickness borosilicate glass slide, also with radiation transmission of >85% in the range of 340–380 nm.

A fluorescent UV lamp (18 W, Royal Philips, Amsterdam, Netherlands) was used for the testing at an intensity of 0.25 mW/cm^2 for 8 h. A viability count was performed by dilution and plating on nutrient agar incubated at 37°C for 48 h. More details are reported elsewhere [37].

3. Results and discussion

3.1. Characterization

3.1.1. Field emission gun scanning electron microscopy

The FEG-SEM images shown in **Figure 2** reveal a relatively widespread, homogeneous, and thick deposition of TiO_2 on the digital inkjet-printed tile surface in comparison to the jet-sprayed tile surface, which shows that voids are present. The EDS data confirmed a greater areal extent of coverage by TiO_2 for digital inkjet printing. However, it is significant that the digital inkjet-printed coating exhibits a considerably lower degree of agglomeration than does the jet-sprayed coating. The former can be expected to provide a greater surface area and associated density of photocatalytically active sites. The reason for this difference is the superior dispersion of the TiO_2 powder by the inclusion of a dispersant in the ink, which reduced the formation of soft agglomerates. Further, it is likely that the included organic phases played a key role in the development of this microstructure through separation of the particles and consequent surface exposure during pyrolysis. Consequently, digital inkjet printing can be expected to exhibit a superior photocatalytic performance owing to the greater volume of deposited TiO_2, the extent of areal coverage of the tile, and exposed surface area.

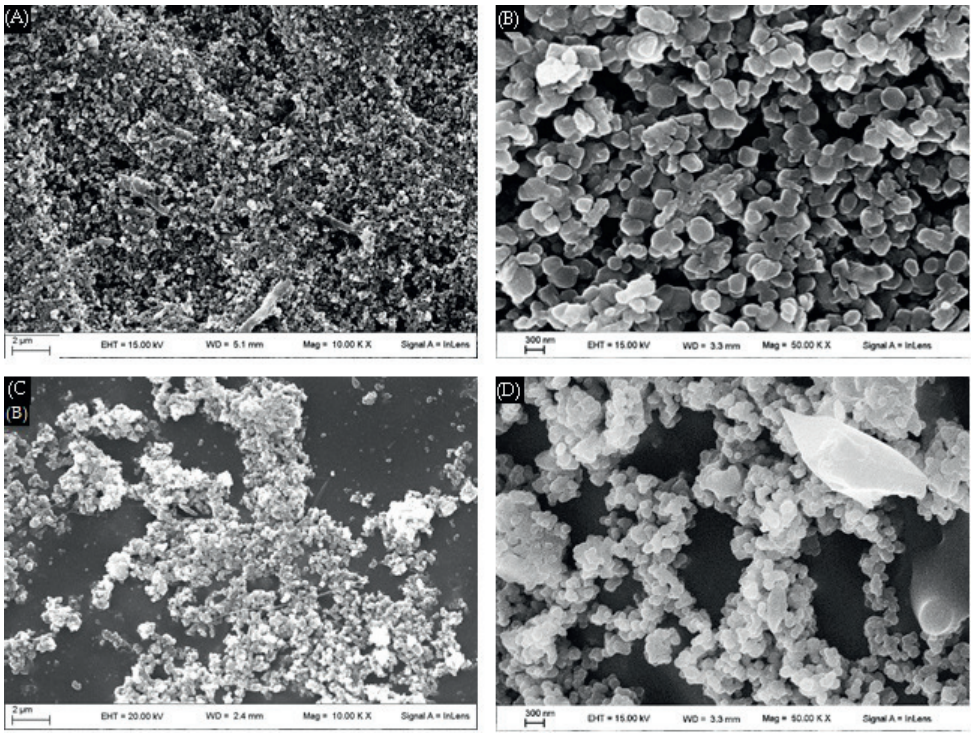

Figure 2. FEG-SEM micrographs digital inkjet-printed coating at (A) low magnification and (B) high magnification and jet-sprayed coating at (C) low magnification and (D) high magnification.

3.1.2. Laser Raman microspectroscopy

In the optical micrographs taken by Raman, shown in **Figure 3**, the lighter rougher regions consist of TiO_2 and the darker regions are the exposed porcelain grès substrates. These images confirm that the TiO_2 deposited by digital inkjet printing is more widespread than that by jet spraying. **Figure 4** shows that the Raman spectra of the digital inkjet-printed and the jet-sprayed coatings are significantly different. The intensities of the peaks and the slopes of the baselines indicate the TiO_2 content of the coating and the glass content, respectively, for each sample. That is, lower peak intensities indicate a low amount of TiO_2 and/or a low degree of crystallinity and the sloped baseline indicates a high glass content in the vitreous tile. The greater peak intensities and flat baseline for the digital inkjet-printed coating confirm the greater extent of coverage of the tile by TiO_2, whereas the low peak intensities and sloped baseline for the jet-sprayed coating confirm the low areal distribution of TiO_2. Since laser Raman microspectroscopy does not analyze amorphous materials accurately, the peak at 510 cm^{-1} is attributed to albite feldspar and the peak at 610 cm^{-1} to α-quartz. The two other small but relatively sharp peaks at 439 and 356 cm^{-1} could not be identified.

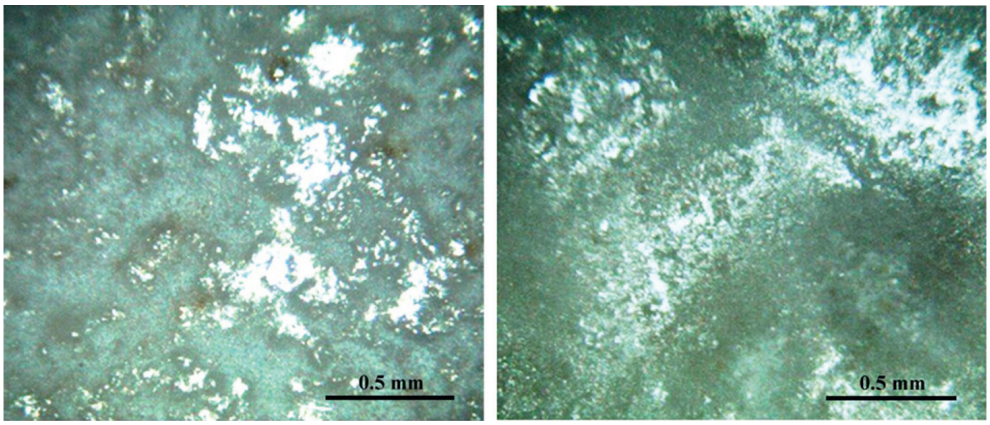

Figure 3. Optical micrographs of (A) digital inkjet-printed coating and (B) jet-sprayed coating.

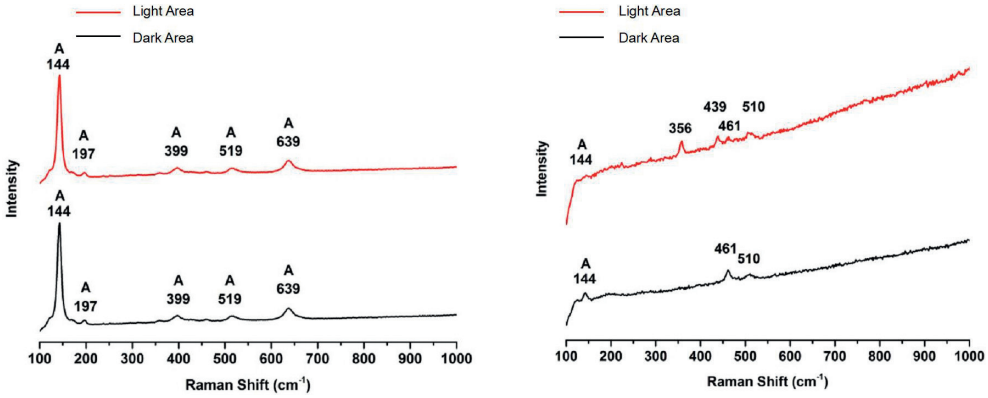

Figure 4. Laser Raman microspectra of (A) digital inkjet-printed coating and (B) jet-sprayed coating.

3.2. Photocatalytic testing

3.2.1. VOC photodegradation

Figure 5 shows the UV photodegradation of ethanol and toluene. Both sets of data demonstrate the superior photocatalytic performance of the digital inkjet-printed coating. While similar testing of Kronos 1077 bulk powder has been shown to decompose ethanol completely in 1 h [37], this work for the deposition of this TiO_2 powder as a digital inkjet-printed coating shows that nearly complete decomposition (~97%) requires 6 h. By contrast, the jet-sprayed coating decomposes only ~47% of the ethanol after 6 h. Interestingly, both coatings outperform the powder when decomposing the more stable aromatic toluene ring. While Kronos 1077 bulk

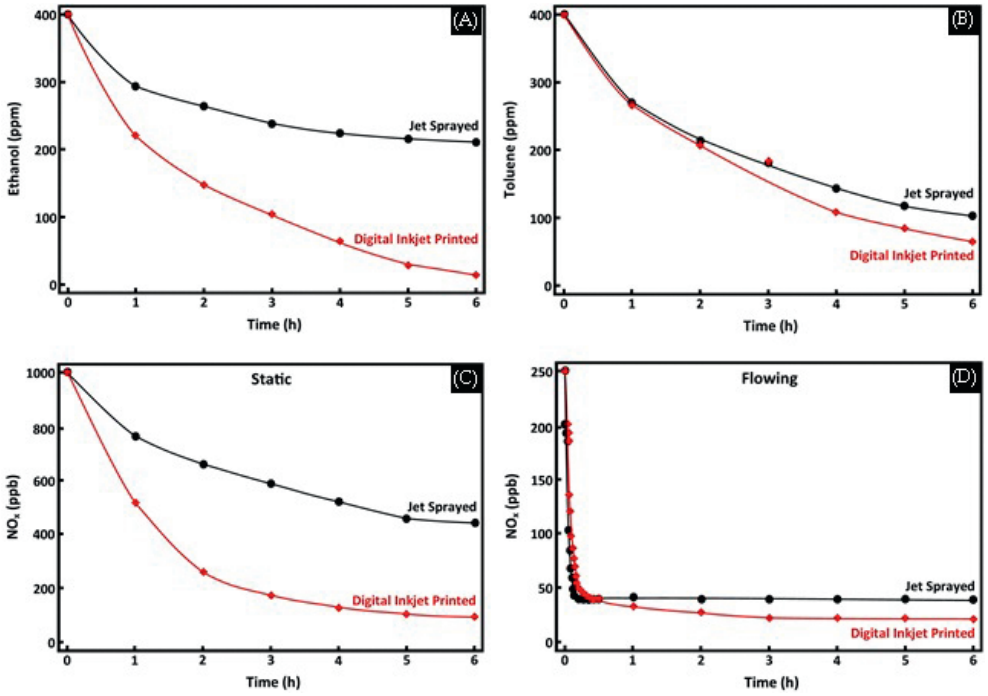

Figure 5. Photodegradation over time by digital inkjet-printed and jet-sprayed coatings of (A) ethanol, (B) toluene, (C) static NO_x, and (D) flowing NO_x.

powder decomposed only ~43% of toluene after 6 h, the digital inkjet-printed coating decomposes ~84% and the jet-sprayed coating decomposes ~75%. It is probable that the difference in results for ethanol and toluene is that while both involved decomposition by photocatalysis, the latter also included a contribution from direct photolysis, which was enhanced by the greater surface area of the coating exposed to UV in comparison to that of a powder bed. This component may be significant because the difference between the two coating techniques is less than that for ethanol photodegradation.

These data confirm that the photocatalytic performance of the digital inkjet-printed coating is superior to that of the jet-sprayed coating for VOC decomposition. This is a result of the greater extent of coverage, more even areal distribution, a reduced agglomeration, a greater extent of exposed particle surface area, and a greater crystallinity of the TiO_2 in the digital inkjet-printed coating.

3.2.2. NO_x photodegradation

Figure 5 also shows the UV photodegradation of NO_x in both batch and continuous-flow reactors. Again, the digital inkjet-printed coating outperforms the jet-sprayed coating. After 6 h under static conditions, the digital inkjet-printed coating decomposes ~90% of the NO_x

while the jet-sprayed coating decomposes only ~56%. After 6 h under flowing conditions, the performances were closer, with the digital inkjet-printed and jet-sprayed coatings decomposing ~80 and ~74% of the NO_x, respectively. It is clear that the maximal levels of decomposition were attained relatively quickly and they were maintained such that no deactivation was observed.

The larger dimensions (60 × 60 cm) of the tiles and the lower NO_x concentration used during the testing under flowing conditions provide a better simulation of real environmental conditions [40]. It may be noted that this digital inkjet-printing technology is capable of coating dimensions as large as 150 by 300 cm.

3.3. Antibacterial testing

Table 1 summarizes the results of the antibacterial testing, which reveals that both types of coatings were highly effective in destroying *E. coli* (gram-negative), which is part of the bacterial flora of human and animal intestines and hence a suitable indicator of potential contamination of drinking water and food. These data show that UV irradiation alone is capable of destroying ~45–72% of the bacteria while both photocatalytic coatings destroy essentially all of the bacteria. After photocatalysis (R_L), the digital inkjet-printed and jet-sprayed coatings are essentially equivalent. However, with photocatalysis (ΔR), the digital inkjet-printed coating clearly outperforms the jet-sprayed coating. Hence, these data are in basic agreement with those for the photodegradation of ethanol and toluene. However, they must be interpreted in light of the different surface topographies, where **Figures 2** and **3** show that the jet-sprayed coating provides less homogeneous coverage and hence presents a more

Antibacterial activity of photocatalytic coatings using E. coli ATCC 8739				
Symbol	**Parameter**	**Units**	**Uncoated tile 1**	**Uncoated tile 2**
Uncoated porcelain grès tile controls				
N	Number of live bacteria	Cells	1,900,000	1,100,000
A	Number of live bacteria after inoculation	Cells/mL	280,000	160,000
B_D	Number of live bacteria before UV irradiation	Cells/mL	220,000	600,000
B_L	Number of live bacteria after UV irradiation	Cells/mL	120,000	170,000
—	Reduction in bacterial count after UV irradiation	%	45.45	71.67
TiO_2-coated porcelain grès tiles				
Symbol	**Parameter**	**Units**	**Digital inkjet-printed tile**	**Jet-sprayed tile**
C_D	Number of live bacteria before photocatalysis	Cells/mL	180,000	130,000
C_L	Number of live bacteria after photocatalysis	Cells/mL	10	10
—	Reduction in bacterial count after photocatalysis	%	99.99	99.99
R_L	Antibacterial activity after photocatalysis	—	4.1	4.2
ΔR	Antibacterial activity with photocatalysis	—	4.1	3.6

Table 1. Summary of the antibacterial testing results on sprayed and digital printed tiles.

uneven surface that is likely to be more amenable to cell attachment and proliferation [41]. A second factor is the sizes of the species that were examined, where **Table 2** [42, 43] contextualizes the view that the photocatalytic performance is correlated through size similarities between the photocatalyst and the species [42].

$$R_L = \log_{10}(B_L/C_L) \tag{1}$$

$$\Delta R = \log_{10}(B_L/C_L) - \log_{10}(B_D/C_D) \tag{2}$$

3.4. Life cycle assessment

In 1993, the Society of Environmental Toxicology and Chemistry (SETAC) standardized the process for life cycle assessment (LCA) to include four components: (1) goal and scope, (2) inventory, (3) impact assessment, and (4) data interpretation [44]. LCA normally is applied to early-stage plants in order to investigate environmental hot spots arising from new technologies [45] or to establish industrial-scale processes for the comparison of divergent designs and optimization of environmental profiles [46]. In this work, the LCA has been modeled for the production of photocatalytic ceramic tiles by digital inkjet printing and jet spraying.

The approach applies *gate-to-gate* boundaries using a functional unit of 1 m^2 of tiles produced in Modena, Italy. *SimaPro* (Version 8.3.0.0) extracted the secondary data from the *Ecoinvent 3* database. *ILCD 2011 Midpoint +* (Version 1.08) and *IPCC 2013 GWP 100a* methods were used to calculate the impacts, which are given in terms of micro-eco-points (μPt). An eco-point is defined as one thousandth of the total environmental impact caused by a statistical European citizen per year [47]. The LCA was done in accordance with the *ISO/TC 207/SC 5 Life Cycle Assessment* methodologies for the principles and framework as well as the requirements and guidelines. For the inventory phase, these two processes were divided into substeps.

In order to highlight the differences between the two production processes, LCA comparison calculations were performed using the *ILCD 2011 Midpoint +* method, weighting the results for the 16 impact categories that were considered. **Figure 6** shows the results graphically and **Table 3** lists them numerically.

Species	Size (nm)	Reference
Ethanol	0.437	[43]
Toluene	0.564	[43]
E. coli	1000 × 3000*	[42]
Viruses	10–300	[42]
Bacteria	500–5000	[42]
Fungi	5000–15,000	[42]

*Rod-like shape.

Table 2. Sizes of tested and other relevant species.

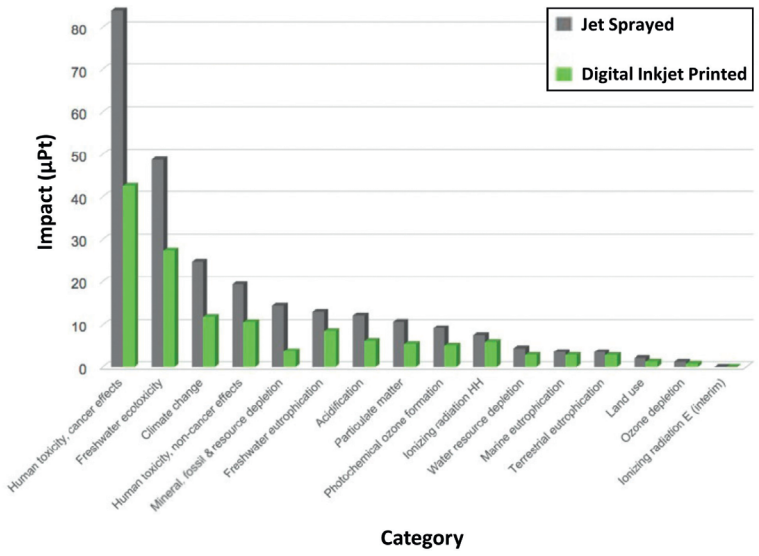

Figure 6. Graphical data for impact (µPt) assessments of digital inkjet-printed and jet-sprayed coatings.

Impact category	Jet sprayed	Digital inkjet printed	Difference (%)
Human toxicity, cancer effects	83.83	42.49	49.31
Freshwater ecotoxicity	48.74	27.41	43.76
Climate change	24.68	11.82	52.11
Human toxicity, non-cancer effects	19.35	10.62	45.10
Mineral, fossil and resource depletion	14.44	3.69	74.41
Freshwater eutrophication	12.99	8.36	35.62
Acidification	12.14	6.13	49.50
Particulate matter	10.70	5.40	49.56
Photochemical ozone formation	9.17	5.04	45.03
Ionizing radiation, human health	7.44	5.85	21.42
Water resource depletion	4.38	2.76	36.90
Marine eutrophication	3.52	2.77	21.36
Terrestrial eutrophication	3.48	2.75	20.95
Land use	2.04	1.18	42.40
Ozone depletion	1.16	0.70	39.99
Ionizing radiation, ecosystems (interim)	0.00	0.00	0.00

Table 3. Numerical data for impact (µPt) assessments of digital inkjet-printed and jet-sprayed coatings.

These data show that jet spraying makes consistently greater impacts than digital inkjet printing does, with the most significant impacts being on human toxicity, cancer effects, freshwater ecotoxicity, and climate change. The first two of these categories have been examined in more detail using *USEtox* calculations and the third category also has been examined using *IPCC 110a* calculations. These analyses reveal that their impacts derive almost entirely from the energy required by the production processes. This explains why jet spraying projects very high impact values since this process also is relatively energy-intensive. It is notable that the impacts of climate change and mineral, fossil and resource depletion reveal differences of >50% between the two production methods. Again, these significant differences are attributed to energy requirements. Three other categories (human toxicity, cancer effects, acidification, and particulate matter) also show nearly the same differential of ~50%. The single-score analysis, which is the average of all values in the 16 categories, shows that digital inkjet printing is ~46% lower than jet spraying.

Further, the calculation of the CO_2 equivalents, carried out by the *IPCC 100a* method, demonstrates that jet spraying has a greater impact than digital inkjet printing by a difference of 3.42 kg CO_2 versus 1.63 kg CO_2. A final point of difference is that the application of the *ILCD* method reveals that NO_x production demonstrates the same trend, with 2.10 g NO_x from jet spraying and 1.65 g NO_x from digital inkjet printing.

The preceding LCA data suggest that the traditional method of jet spraying is considerably inferior to that of digital inkjet printing and that further detailed analysis of each step of the process is likely to improve the process and its outcomes commercially, environmentally, and performatively.

4. Conclusions

This work reports design, synthesis, and characterization of photocatalytic TiO_2-coated tiles fabricated by the conventional jet spraying technique and the new technique of digital inkjet printing. The latter represents a significant improvement over the former, in that (1) it provides a more precise deposition as it utilizes piezoelectric heads to direct the suspension within an electrostatic field, (2) the microsized TiO_2 powder strikes a medium that balances the small size advantageous for photocatalytic performance and the ability to resist solubility in the glass bonding to the tile against the large size that inhibits respirability, and (3) the topography of the digital inkjet-printed coating is less amenable to cell attachment and proliferation than those of the jet-sprayed coating.

The performance data show that the digital inkjet-printed coating was significantly more effective than the jet-sprayed coating in ethanol photodegradation. While the same trend was observed for toluene photodegradation, the difference was not as significant owing to direct photolysis of this aromatic compound. Both coatings were highly effective in destroying E. coli but the antibacterial activity with photocatalysis (ΔR) of the digital inkjet-printed coating was significantly superior to that of the jet-sprayed coating. Similarly, the LCA analysis of the impact assessments reveals the multifarious advantages of the digital inkjet-printed tile.

Acknowledgements

In memory of Benedetta Sacchi, a worthy researcher and a collaborator for years of the UNIMI research group. The authors would like to thank Dr. A. Carletti (Artest, Italy) for the antibacterial testing and Mr. R. Pellini (GranitiFiandre, Italy) for the preparation of the photocatalytic tiles. This research was supported financially by the *LIFE+ Environment Policy and Governance* project *Digitalife LIFE13 ENV/IT/000140*. The UNSW authors acknowledge the characterization facilities provided by the Mark Wainwright Analytical Centre, UNSW Sydney, Australia.

Author details

Claudia L. Bianchi[1]*, Carlo Pirola[1], Marta Stucchi[1], Giuseppina Cerrato[2], Federico Galli[1], Alessandro Di Michele[3], Serena Biella[1], Wen-Fan Chen[4], Pramod Koshy[4], Charles Sorrell[4] and Valentino Capucci[5]

*Address all correspondence to: claudia.bianchi@unimi.it

1 Dipartimento di Chimica, Università di Milano, Italy

2 Dipartimento di Chimica, Università di Torino, Italy

3 Dipartimento di Fisica e Geologia, Università di Perugia, Italy

4 School of Materials Science and Engineering, UNSW Sydney, Australia

5 GranitiFiandre Group, Italy

References

[1] Prüss-Ustün A, Wolf J, Corvalán C, Bos R, Neira M. Preventing Disease through Healthy Environments: A Global Assessment of the Burden of Disease from Environmental Risks. Geneva, Switzerland: World Health Organization (WHO); 2016

[2] Anonymous. Ambient Air Pollution: A Global Assessment of Exposure and Burden of Disease. Geneva, Switzerland: World Health Organization (WHO); 2016

[3] Martin WJ II, Glass RI, Araj H, Balbus J, Collins FS, Curtis S, Diette GB, Elwood WN, Falk H, Hibberd PL, Keown SEJ, Mehta S, Patrick E, Rosenbaum J, Sapkota A, Tolunay HE, Bruce NG. Household air pollution in low- and middle-income countries: Health risks and research priorities. PLOS Medicine. 2013;**10**:paper 1001455 (8 pp)

[4] Tefera W, Asfaw A, Gilliland F, Worku A, Wondimagegn M, Kumie A, Samet J, Berhane K. Indoor and outdoor air pollution—Related health problem in Ethiopia: Review of related literature. Ethiopian Journal of Health Development. 2016;**30**(special issue):5-16

[5] Chen A, Cao Q, Zhou J, Yang B, Chang V, Nazaroff WW. Indoor and outdoor particles in an air-conditioned building during and after the 2013 haze in Singapore. Building and Environment. 2016;**99**:73-81

[6] Phoothiwut S, Junyapoon S. Size distribution of atmospheric particulates and particulate-bound polycyclic aromatic hydrocarbons and characteristics of PAHs during haze period in Lampang Province, Northern Thailand. Air Quality, Atmosphere and Health. 2013;**6**:397-405

[7] Beelen R, Hoek G, Vienneau D, Eeftens M, Dimakopoulou K, Pedeli X, Tsai M-Y, Künzli N, Schikowski T, Marcon A, Eriksen KT, Rasschou-Nielsen O, Stephanou E, Patelarou E, Lanki T, Yli-Tuomi T, Declercq C, Falq G, Stempfelet M, Birk M, Cyrys J, von Klot S, Nádor G, Varró MJ, Dėdelė A, Gražulevičienė R, Mölter A, Lindley S, Madsen C, Cesaroni G, Ranzi A, Badaloni C, Hoffmann B, Nonnemacher M, Krämer U, Kuhlbusch T, Cirach M, de Nazelle A, Nieuwenhuijsen M, Bellander T, Korek M, Olsson D, Strömgren N, Dons E, Jerrett M, Fisher P, Wang M, Brunekreef B, de Hoogh K. Development of NO_2 and NO_x land use regression models for estimating air pollution exposure in 36 study areas in Europe–The ESCAPE project. Atmospheric Environment. 2013;**72**:10-23

[8] Environmental Protection Agency (EPA). https://cfpub.epa.gov/roe/chapter/air/indoorair.cfm

[9] Dales R, Liu L, Wheeler AJ, Gilbert NL. Quality of indoor residential air and health. CMAJ·JAMC. 2008;**179**:147-152

[10] American Lung Association. http://www.lung.org/stop-smoking/smoking-facts/

[11] Ren H, Koshy P, Chen W-F, Qi S, Sorrell CC. Photocatalytic materials and technologies for air purification. Journal of Hazardous Materials. 2017;**325**:340-366

[12] Fujishima A, Zhang X, Tryk DA. TiO_2 photocatalysis and related surface phenomena. Surface Science Reports. 2008;**63**:515-582

[13] Bak T, Nowotny J, Rekas M, Sorrell CC. Photo-electrochemical hydrogen generation from water using solar energy. Materials-related aspects. International Journal of Hydrogen Energy. 2002;**27**:991-1022

[14] Fujishima A, Nakata K, Ochiai T, Manivannan A, Tryk DA. Recent aspects of photocatalytic technologies for solar fuels, self-cleaning, and environmental cleanup. Electrochemical Society Interface. 2013;**22**:51-56

[15] Chong MN, Jin B, Chow CWK, Saint C. Recent developments in photocatalytic water treatment technology: A review. Water Research. 2010;**44**:2997-3027

[16] Chen J, Poon C-S. Photocatalytic construction and building materials: From fundamentals to applications. Building and Environment. 2009;**44**:1899-1906

[17] Fujishima A, Zhang X. Titanium dioxide photocatalysis: Present situation and future approaches. Comptes Rendus Chimie. 2006;**9**:750-760

[18] Gagliardi M. Photocatalysts: Technologies and Global Markets. Market Research Report AVM069B. Wellesley, MA, USA: BCC Research LLC; 2015

[19] Poon CS, Cheung E. NO removal efficiency of photocatalytic paving blocks prepared with recycled materials. Construction and Building Materials. 2007;**21**:1746-1753

[20] Hüsken G, Hunger M, Brouwers HJH. Comparative study on cementitious products containing titanium dioxide as photo-catalyst. In: Baglioni P, Cassar L, editors. International RILEM Symposium on Photocatalysis, Environment and Construction Materials. Bagneux, France: RILEM Publications; 2007. pp. 147-154

[21] Strini A, Cassese S, Schiavi L. Measurement of benzene, toluene, ethylbenzene and o-xylene gas phase photodegradation by titanium dioxide dispersed in cementitious materials using a mixed flow reactor. Applied Catalysis B: Environmental. 2005;**61**:90-97

[22] Demeestere K, Dewulf J, De Witte B, Beeldens A, Van Langenhove H. Heterogeneous photocatalytic removal of toluene from air on building materials enriched with TiO_2. Building and Environment. 2008;**43**:406-414

[23] Rachel A, Subrahmanyam M, Boule P. Comparision of photocatalytic efficiencies of TiO_2 in suspended and immobilised form for the photocatalytic degradation of nitrobenzenesulfonic acids. Applied Catalysis B: Environmental. 2002;**37**:301-308

[24] Yu JC-M. Deactivation and Regeneration of Environmentally Exposed Titanium Dioxide (TiO_2) Based Products. Departmental Order Ref. No.: E183413. Chinese University of Hong Kong, Hong Kong: Environmental Protection Department, HKSAR; 2003

[25] Auvinen J, Wirtanen L. The influence of photocatalytic interior paints on indoor air quality. Atmospheric Environment. 2008;**42**:4101-4112

[26] Wang J, Chen C, Liu Y, Jiao F, Li W, Lao F, Li Y, Li B, Ge C, Zhou G, Gao Y, Zhao Y, Chai Z. Potential neurological lesion after nasal instillation of TiO_2 nanoparticles in the anatase and rutile crystal phases. Toxicology Letters. 2008;**183**:72-80

[27] Radeka M, Markov S, Lončar E, Rudić O, Vučetić S, Ranogajec J. Photocatalytic effects of TiO_2 mesoporous coating immobilized on clay roofing tiles. Journal of the European Ceramic Society. 2014;**34**:127-136

[28] Powell MJ, Quesada-Cabrera R, Taylor A, Teixeira D, Papakonstantinou I, Palgrave RG, Sankar G, Parkin IP. Intelligent multifunctional VO_2/SiO_2/TiO_2 coatings for self-cleaning, energy-saving window panels. Chemistry of Materials. 2016;**28**:1369-1376

[29] Martinet C, Paillard V, Gagnaire A, Joseph J. Deposition of SiO_2 and TiO_2 thin films by plasma enhanced chemical vapor deposition for antireflection coating. Journal of Non-Crystalline Solids. 1997;**216**:77-82

[30] De Falco G, Porta A, Del Gaudio P, Commodo M, Minutolo P, D'Anna A. Antimicrobial activity of TiO_2 coatings prepared by direct thermophoretic deposition of flame-synthesized nanoparticles. Nanomater. 2017;**2**:1493-1498

[31] Jafari H, Afshar S, Zabihi O, Naebe M. Enhanced photocatalytic activities of TiO_2–SiO_2 nanohybrids immobilized on cement-based materials for dye degradation. Research on Chemical Intermediates. 2016;**42**:2963-2978

[32] Calia A, Lettieri M, Masieri M, Pal S, Licciulli A, Arima V. Limestones coated with photocatalytic TiO_2 to enhance building surface with self-cleaning and depolluting abilities. Journal of Cleaner Production. 2017;**165**:1036-1047

[33] Tobaldi DM, Graziani L, Seabra MP, Hennetier L, Ferreira P, Quagliarini E, Labrinch JA. Functionalised exposed building materials: Self-cleaning, photocatalytic and biofouling abilities. Ceramics International. 2017;**43**:10316-10325

[34] Morita N, Khalate AA, van Buul AM, Wijshoff H. Inkjet printheads. In: Hoath SD, editor. Fundamentals of Inkjet Printing: The Science of Inkjet and Droplets. Weinheim, Germany: Wiley-VCH Verlag GmbH & Co. KGaA; 2016

[35] Bianchi CL, Pirola C, Galli F, Stucchi M, Morandi S, Cerrato G, Capucci V. Nano and micro-TiO_2 for the photodegradation of ethanol: Experimental data and kinetic modelling. RSC Advances. 2015;**5**:53419-53425

[36] Bianchi CL, Gatto S, Pirola C, Naldoni A, Di Michele A, Cerrato G, Crocellà V, Capucci V. Photocatalytic degradation of acetone, acetaldehyde and toluene in gas-phase: Comparison between nano and micro-sized TiO_2. Applied Catalysis B: Environmental. 2014;**146**: 123-130

[37] Bianchi CL, Pirola C, Stucchi M, Sacchi B, Cerrato G, Morandi S, Di Michele A, Carletti A, Capucci V. A new frontier of photocatalysis employing micro-sized TiO_2: Air/water pollution abatement and self-cleaning/antibacterial applications. In: Semiconductor Photocatalysis—Materials, Mechanisms and Applications. Cao, W. ed. InTech, London, UK, Chapter 23. 2016

[38] Bianchi CL, Stucchi M, Pirola C, Cerrato G, Morandi S, Sacchi B, Vitali S, Di Michele A, Capucci V. Micro-sized TiO_2 catalyst in powder form and as coating on porcelain grès tile for the photodegradation of phenol as model pollutant for water phase. Advances in Materials Science. 2017;**2**:1-6

[39] Bianchi CL, Pirola C, Galli F, Cerrato G, Morandi S, Capucci V. Pigmentary TiO_2: A challenge for its use as photocatalyst in NO_x air purification. Chemical Engineering Journal. 2015;**261**:76-82

[40] Bianchi CL, Pirola C, Galli F, Vitali S, Minguzzi A, Stucchi M, Manenti F, Capucci V. NO_x degradation in a continuous large-scale reactor using full-size industrial photocatalytic tiles. Catalysis Science & Technology. 2016;**6**:2261-2267

[41] Deligianni DD, Katsala ND, Koutsoukos PG, Missirlis YF. Effect of surface roughness of hydroxyapatite on human bone marrow cell adhesion, proliferation, differentiation and detachment strength. Biomaterials. 2001;**22**:87-96

[42] Blake DM, Maness P-C, Huang Z, Wolfrum EJ, Huang J, Jacoby WA. Application of the photocatalytic chemistry of titanium dioxide to disinfection and the killing of cancer cells. Separation and Purification Methods. 1999;**28**:1-50

[43] Marcus Y. The sizes of molecules–Revisited. Journal of Physical Organic Chemistry. 2003; **16**:398-408

[44] Klöpffer W. The role of SETAC in the development of LCA. International Journal of Life Cycle Assessment. 2006;**11**(Suppl. 1):116-122

[45] Galli F, Pirola C, Previtali D, Manenti F, Bianchi CL. Eco design LCA of an innovative lab scale plant for the production of oxygen-enriched air. Comparison between economic and environmental assessment. Journal of Cleaner Production. 2018;**171**:147-152

[46] Curran MA. Life cycle assessment: A review of the methodology and its application to sustainability. Current Opinion in Chemical Engineering. 2013;**2**:273-277

[47] Grzesik K, Usarz M. A life cycle assessment of the municipal waste management system in Tarnów. Geomatics and Environmental Engineering. 2016;**10**:29-38